

# The effects of silica-coated $Y_2O_2S:Eu^{3+}$ red phosphor on the lighting properties of the light-emitting diode

Phuc Dang Huu<sup>1</sup>, Phan Xuan Le<sup>2</sup>

<sup>1</sup>Faculty of Fundamental Science, Industrial University of Ho Chi Minh City, Ho Chi Minh City, Vietnam

<sup>2</sup>Faculty of Mechanical-Electrical and Computer Engineering, School of Engineering and Technology, Van Lang University, Ho Chi Minh City, Vietnam

## Article Info

### Article history:

Received Jun 9, 2021

Revised Apr 28, 2022

Accepted Jun 1, 2022

### Keywords:

Color uniformity

Luminous flux

Mie-scattering theory

$Y_2O_2S:Eu^{3+}$

## ABSTRACT

The red phosphor  $Y_2O_2S:Eu^{3+}$  coated with silica ( $SiO_2$ ) nanocomposite was synthesized using the sol-gel method with dip-coating technique. The purpose of coating the poly (methyl methacrylate) (PMMA)- $SiO_2$  composite on  $Y_2O_2S:Eu^{3+}$  phosphor's surface is to protect the phosphor and improve its scattering ability. The three primary ingredients of coating composition include methyl methacrylate (MMA) monomer, tetraethyl orthosilicate (TEOS), and  $SiO_2$  nanoparticles. Via Mie scattering theory, the scattering of  $SiO_2$  is examined, which primarily determines the scattering of PMMA- $SiO_2$ -coated  $Y_2O_2S:Eu^{3+}$ . The larger particles of  $SiO_2$  in the coating composite leads to better scattering properties. When being applied in the dual-film remote phosphor configuration of a LED,  $SiO_2@Y_2O_2S:Eu^{3+}$  considerably enhances the CRI and the color quality scale (CQS). The highest CRI and CQS can be observed at approximately 85 and 74 with 23 %wt. and 26 %wt. the concentration of  $SiO_2@Y_2O_2S:Eu^{3+}$ , respectively. Nevertheless, the illuminating beam of the package gradually declines as the concentration of  $SiO_2@Y_2O_2S:Eu^{3+}$  go up, which might be ascribed to excessive scattering occurrences in the double-layer remote package.

This is an open access article under the [CC BY-SA](https://creativecommons.org/licenses/by-sa/4.0/) license.



## Corresponding Author:

Phuc Dang Huu

Faculty of Fundamental Science, Industrial University of Ho Chi Minh City

No. 12 Nguyen Van Bao Street, Ho Chi Minh City, Vietnam

Email: danghuuphuc@iuh.edu.vn

## 1. INTRODUCTION

Phosphor materials have been utilized in fabricating white light-emitting diodes (WLEDs) and have drawn significant researchers' attention and manufacturers in this illumination aspect. The benefits of WLED using phosphor conversion technology can be listed as durability, energy savings, affordable maintenance, and enhanced safety [1], [2]. Thus, WLED is more favorable to advance illuminating application than the conventional halogen or incandescent lights. Commonly, a criterion white LED is produced with a GaN-based LED chip that emits blue light employing phosphor YAG:Ce emits yellow light. Nonetheless, several studies presented major drawbacks due to two-color mixing of the conventional structure combining a blue-color LED die and a film of phosphor that emits yellow light, including chromatic shift and inferior CRI (about 60–70) [3]-[5]. Generally, the solution is to investigate white LEDs constitutive from fundamental colors of blue, red, and green (RGB). A white LED can be made by precoating the phosphor combination of RGB phosphors above a ultraviolet (UV) LED die, or phosphors emit green and red light above a blue-color LED chip [6]-[8]. The favorable RGB phosphors for tricolor close-UV Indium gallium nitride-light-emitting diode (InGaN-LED) chips were  $Y_2O_2S:Eu^{3+}$ , ZnS, and  $BaMgAl_{10}O_{17}Eu^{2+}$  [9], [10]. Unfortunately, the red phosphor  $Y_2O_2S:Eu^{3+}$  exhibits lower photoluminescence (PL) intensity than the other green and blue ones, leading to the need for a

combination of phosphor with a huge number of red phosphors for proper hue rendering performance. Besides, due to its instability, the endurance of  $Y_2O_2S:Eu^{3+}$  under close-UV irradiation is deficient. It is now advised that the challenges with red phosphor materials should be resolved for WLEDs to improve [11]-[13]. Several efforts were made for the purpose of addressing the limitations of the  $Y_2O_2S:Eu^{3+}$  red phosphor. When several alkaline earth sulfides were combined with rare-earth ion activators, this combination outperformed  $Y_2O_2S:Eu^{3+}$  red phosphors [14]-[16]. However, because of the inefficient moisture resistance and instability to other atmospheric elements, the usage of alkaline earth sulfides has been restricted. The results are still insufficient, although several studies are being conducted to improve the efficacy and resistance features of alkaline earth sulfides by modifying their composition and fabrication processes. For display devices and LEDs, phosphor particles are frequently covered using oxides including silica,  $Y_2O_3$ , ZnO, MgO, and organic polymers. Phosphor adherence to glass substrates has improved thanks to coatings, which also offers the phosphor great moisture resistance and durability, as well as protects the phosphor from being degraded when affected by UV irradiation [17]-[19].

To minimize the PL intensity loss, it is crucial to get a transparent coating with a specific amount uniformly covering the surface of each phosphor particle. About the stability, a layer-like uniform layout might be preferred over an island-like non-uniform covering. As a film-like uniform covering could be performed with littler grains having even size, it is recommended to use monodispersed nanoparticles that do not present aggregate formation as an alternative phosphor covering. We employed a dip-covering procedure with a sol-gel procedure to cover silica nanoparticles on the phosphor surface. Then, the poly(methylmethacrylate) (PMMA)-silica nanocomposite can be used to cover the phosphor surface by reacting methylmethacrylate (MMA) monomer with tetraethyl orthosilicate (TEOS). The Mie-scattering was applied to carry out the scattering analysis of the  $SiO_2$  particles, which also determined the scattering effects of the coted red phosphor on the light properties of the WLED packages. The impacts of  $SiO_2@Y_2O_2S:Eu^{3+}$  on the double layer phosphor configuration are demonstrated via the color rendering metrics and luminous features.

## 2. METHOD

### 2.1. Materials and procedures

The Stober sol-gel process was used to create nearly mono-disperse and spherical silica particles. The experiment lasted one hour and was conducted at various temperatures. The quantities concerning reactants (TEOS and water), catalyst (ammonium hydroxide), temperature, and reaction media all influence the diameter of silica nanoparticles. Particle size decreased as TEOS and  $NH_4OH$  concentrations decreased while water concentrations increased. When the particle diameter of  $SiO_2$  was over 25 nm, virtually monodisperse and spherical nanoparticles were generated. Meanwhile, aggregation formation was seen with  $SiO_2$  nanoparticles smaller than 25 nm. Thus, we have to modify the temperature and medium of the reaction to prevent unwanted aggregate formation. The MMA monomer was then introduced to the reaction with TEOS to create an even coating film above the  $Y_2O_2S:Eu^{3+}$  red phosphor. A high-resolution transference electron microscope (Japan) was used to examine the geometries of  $SiO_2$  nanoparticles and  $Y_2O_2S:Eu^{3+}$  phosphors before and after coating. In addition, the median magnitude of a particle in each specimen was determined by analyzing 10 TEM pictures of 10 different specimens with image analysis software (Korea). An FTIR spectrometer–Fourier transform infrared spectrometer (USA) and an EDS–energy dispersive spectroscopy (England) was used to validate phosphor with PMMA-silica surface coating. The photoluminescence (PL) can be measured at 30 °C using a monochromatic and photomultiplier detector (Korea). Recording all of the PL spectra was given at 1 nm bandwidths at the emitting slit. Five samples of each phosphor were prepared for the PL experiment. After testing in duplicate, the outcomes of the phosphors were averaged. Variations in cathode luminescence (CL) with aging period were explored for the long-term steadiness assessment of the phosphors using a bombardment 10 kV beam of electrons with a mean current density of  $45 \mu A/cm^2$  for 30 minutes. Furthermore, for the tests of heat stabilization and moisture resistance of the phosphor specimens with and without PMMA-silica coating, the phosphor specimens were aged in a heat-controlled humidity chamber (Korea) at 100 °C and 80% relative humidity, followed by the test on PL strength changing with the aging period.

### 2.2. Simulation

As shown Figure 1(a) and Figure 1(b) presents in detail the WLED simulation with a double-layer remote phosphor design. The use of the LightTools 9.0 illumination design software and Mie scattering theory in this work allows simply simulating WLEDs with dual-layer phosphor structures by analyzing phosphor particle scattering [20], [21]. Then, based on the scattering findings, we can determine the impact of the  $SiO_2@Y_2O_2S:Eu^{3+}$  phosphor on the optic properties of the double-layer phosphor WLED packages at high correlated temperatures of 7700 K - 8500 K. For the double-layer remote phosphor configuration of WLEDs to

work properly, the  $\text{SiO}_2@\text{Y}_2\text{O}_2\text{S:Eu}^{3+}$  film is put over the yellow  $\text{YAG:Ce}^{3+}$  one, as shown Figure 1(c) and Figure 1(d). As a result, the phosphor configuration of WLEDs includes the  $\text{SiO}_2@\text{Y}_2\text{O}_2\text{S:Eu}^{3+}$  phosphor, the yellow phosphor  $\text{YAG:Ce}^{3+}$ , and silicone glues.

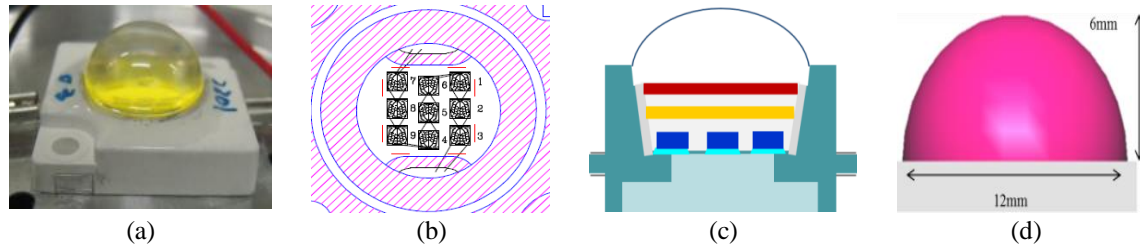


Figure 1. Picture of WLEDs configuration (a) the WLED device, (b) binding graph, (c) illustration of pc-WLEDs model, and (d) simulation of WLEDs utilizing LightTools commercial program

### 2.3. Scattering computation

It was observed that the particle size of  $\text{SiO}_2$  changed depending on the reaction temperature. Particularly, when increasing the reaction temperature, the particles' magnitude declined before stabilizing. At the reaction temperature of about  $30^\circ\text{C}$ , monodisperse  $\text{SiO}_2$  nanoparticles with 50 nm particle size were formed. However, when that temperature increased to over  $80^\circ\text{C}$ , the particle magnitude fell down to roughly 10 nm. Bigger particles (at least 30 nm) generated nearly monodisperse and spherical nanoparticles. It is worth noting that aggregates formed when primary silica nanoparticles smaller than 20 nm were present. There are various plausible explanations for these findings. For example, additional particles are formed when smaller particles are generated. Because tiny particles have a greater outside tension than huge particles, they mix faster to create a more solid surface. As a result, primary silica particles with sizes smaller than around 20 nm produced a network formation due to aggregation, whereas spherical particles with diameters higher than 20 nm produced a spherical structure without aggregation. Increasing the water concentration lowered the diameter of silica nanoparticles from 50 to 10 nm at a reaction heat  $30^\circ\text{C}$ – $80^\circ\text{C}$ . When particle diameters were smaller than roughly 20 nm, however, aggregates containing main silica nanoparticles developed. The data demonstrate that greater reaction temperature can get the size of  $\text{SiO}_2$  nanoparticles decreased even further, but solely changing the reaction temperature would not solve the aggregation formation problems.

The scattering properties of the red phosphor  $\text{Y}_2\text{O}_2\text{S:Eu}^{3+}$  are probably influenced when the PMMA- $\text{SiO}_2$  nanocomposite covers its surface. The changes are possibly caused by the scattering ability of the  $\text{SiO}_2$  particles, which fluctuates owing to the particle size modification. In this study, the Mie-scattering theory is utilized to calculate and analyze the dispersing properties of  $\text{SiO}_2$  particles. Relying on Mie-scattering theory [22]-[25], formulas (1)-(3) can be used to compute the dispersing factor  $\mu_{sca}(\lambda)$ , anisotropy factor  $g(\lambda)$ , and decreased dispersing factor  $\delta_{sca}(\lambda)$ :

$$\mu_{sca} = \int N(r)C_{sca}(\lambda, r)dr \quad (1)$$

$$g(\lambda) = 2\pi \int_{-1}^1 p(\theta, \lambda, r)f(r)\cos\theta d\cos\theta dr \quad (2)$$

$$\delta_{sca} = \mu_{sca}(1 - g) \quad (3)$$

While  $N(r)$  represents the dispensation density of diffusional particles ( $\text{mm}^3$ ),  $C_{sca}$  indicates the dispersing cross-sections ( $\text{mm}^2$ ),  $p(\theta, \lambda, r)$ ,  $\lambda$ , and  $r$  are the phase function, the illuminating wavelength (nm), and radius of diffusional particles ( $\mu\text{m}$ ), respectively.  $\theta$  means the dispersing angle ( $^\circ\text{C}$ ), and  $f(r)$  displays the size dispensation function of the diffusional particles in the phosphor package.

As shown Figure 2 and Figure 3, the increase in diameter of  $\text{SiO}_2$  particles boosted the scattering properties. Moreover, the results at the blue light wavelength (450 nm) are higher than that of the yellow one (550 nm), implying that the blue-light absorption could be better. When enhancing the absorption ability of  $\text{Y}_2\text{O}_2\text{S:Eu}^{3+}$  phosphor with PMMA- $\text{SiO}_2$  coating, the red-light proportion converted from the scattered blue lights is likely to increase. It contributes to the improvement in chromaticity of WLED dual-layer distant phosphor packet. Additionally, the scattering enhancement that  $\text{SiO}_2@\text{Y}_2\text{O}_2\text{S:Eu}^{3+}$  red phosphor brings to the

phosphor structure has significant effects on the overall luminous output of the white LED configuration, which will be discussed in the next section.

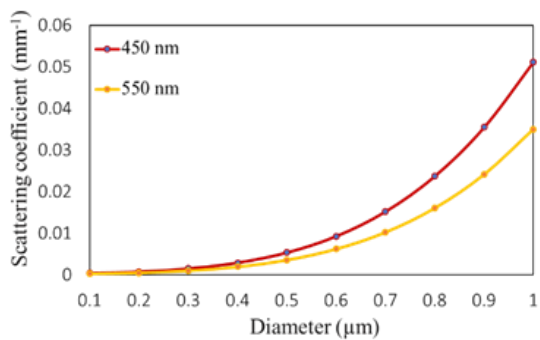


Figure 2. Dispersing factors of  $\text{SiO}_2$  particles at 450 nm and 550 nm

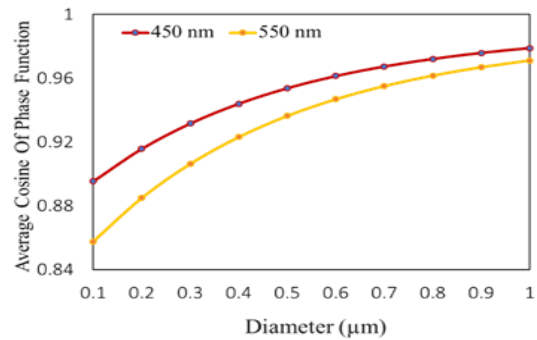


Figure 3. The phase function of  $\text{SiO}_2$  particles at 450 nm and 550 nm

### 3. RESULTS AND DISCUSSION

The influences of the  $\text{SiO}_2$ -coated  $\text{Y}_2\text{O}_2\text{S}:\text{Eu}^{3+}$  on the lighting properties of the WLED employing two remote phosphor layer designs are presented and discussed in this part. Judging the experimental results, the concentration of  $\text{SiO}_2@\text{Y}_2\text{O}_2\text{S}:\text{Eu}^{3+}$  is the main force of the changes in optical performance. The relation between the concentrations of the yellow  $\text{YAG}:\text{Ce}^{3+}$  and  $\text{SiO}_2$ -coated  $\text{Y}_2\text{O}_2\text{S}:\text{Eu}^{3+}$  phosphors will be demonstrated as shown in Figure 4. The remarkable reduction of the yellow-color phosphor weight percentage, at both correlated color temperatures (CCTs) 7700 K and 8500 K. The reduction in yellow phosphor  $\text{YAG}:\text{Ce}^{3+}$  concentration is the result of the scattering enhancement when the  $\text{SiO}_2@\text{Y}_2\text{O}_2\text{S}:\text{Eu}^{3+}$  phosphor is employed. This has two primary benefits to the lighting features of WLEDs, which are the color temperatures consistency and the encourage the reduction of back-scattering that causes light loss in the LED structure. Hence, coating  $\text{SiO}_2$  composite on the red phosphor  $\text{Y}_2\text{O}_2\text{S}:\text{Eu}^{3+}$  enhances both the stability and the scattering of the core phosphor, resulting in improvement of the LED lights.

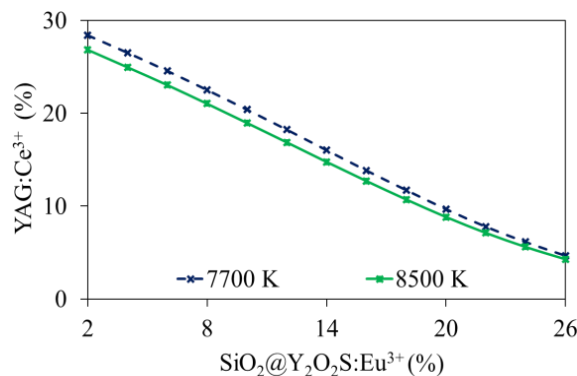


Figure 4. The shift of phosphor concentration occurring to maintain the median CCTs

In terms of the chromaticity of the double-film distant phosphor structure, the CRI and color quality scale (CQS) are investigated. CRI is among the parameters most commonly utilized in the chromatic fidelity test. We can gain a high CRI via enhancing the red energy in the overall spectral emission of the white light. The CRI of the WLED in connection with the concentration of  $\text{SiO}_2@\text{Y}_2\text{O}_2\text{S}:\text{Eu}^{3+}$  is presented as shown in Figure 5. As shown in the picture, the presence of the coated red phosphor is beneficial to the CRI. At the lowest applied concentration (2 %wt), it is possible for the WLED to attain the CRI of 70. Subsequently, increasing the amount of  $\text{SiO}_2@\text{Y}_2\text{O}_2\text{S}:\text{Eu}^{3+}$  content gets the CRI of the structure heightened. The CRI peak can be observed at about 85 with 23 %wt  $\text{SiO}_2@\text{Y}_2\text{O}_2\text{S}:\text{Eu}^{3+}$  in the package. As the concentration surpasses 23 %wt the CRI slightly decreases to 80, which might be caused by the excessive red-light component

leading to color-distribution imbalance. The scattering enhancement offered from the application of  $\text{SiO}_2@Y_2O_2S:Eu^{3+}$  phosphor could be explained for a better CRI. As there are more blue lights scattered, it heightens the change of light mixing between the blue and yellow lights, and thus stimulates the uniformity of the generated light. Moreover, the red phosphors induce the blue-light absorption and convert those blue lights into red lights which is essential to the CRI improvement. Not only the CRI is promoted but also the CQS. National Institute of Standards and Technology's (NIST's) researchers developed CQS in the form of a novel hue rendering metric to overcome the limits of traditional CRI, such as a limited tested color sample. The CQS is believed to be better than the CRI since it evaluates a light source with 15 new color samples; plus, it examines the color coordinate and human visual preference. The CQS changes with the concentration of red phosphor  $\text{SiO}_2@Y_2O_2S:Eu^{3+}$  are demonstrated as shown in Figure 5. Similar to the CRI, the CQS would be proportional to the  $\text{SiO}_2@Y_2O_2S:Eu^{3+}$  concentration. In particular, the higher the mass percentage in  $\text{SiO}_2@Y_2O_2S:Eu^{3+}$  presents, the better the CQS becomes. The CQS peak is about 74 when adding 26 %wt to the phosphor package, see Figure 6. In brief, using the  $\text{SiO}_2@Y_2O_2S:Eu^{3+}$  red phosphor has tremendous advantages to the hue output in the WLED as the scattering properties of original  $Y_2O_2S:Eu^{3+}$  are enhanced with PMMA- $\text{SiO}_2$  coating.

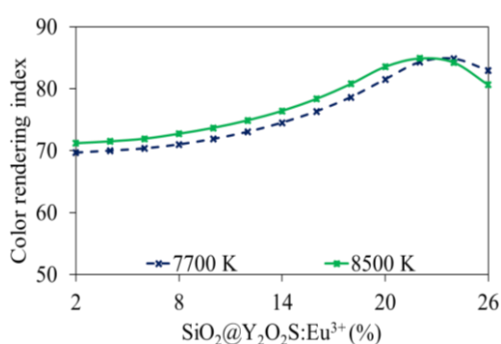


Figure 5. The CRI of WLEDs and  $\text{SiO}_2@Y_2O_2S:Eu^{3+}$  concentration

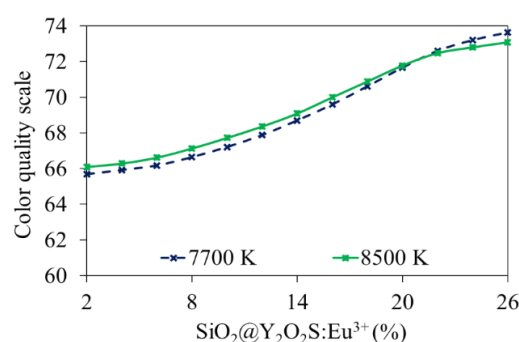


Figure 6. The hue standard scale of WLEDs and  $\text{SiO}_2@Y_2O_2S:Eu^{3+}$  concentration

Last but not least, the luminous efficiency of the WLED with  $\text{SiO}_2@Y_2O_2S:Eu^{3+}$  layer is demonstrated. In contrast to the CRI and the CQS, the lumen output significantly decreases when the content of the  $\text{SiO}_2@Y_2O_2S:Eu^{3+}$  increases, see Figure 7. At 23-26 %wt. the luminous flux is around 400 lm, which is reduced by approximately 600 lm, compared to the figure at 2 %wt  $\text{SiO}_2@Y_2O_2S:Eu^{3+}$ . Therefore, to successfully apply  $\text{SiO}_2@Y_2O_2S:Eu^{3+}$  red phosphor to achieve optical-performance improvement for WLEDs, the consideration and modification of this phosphor concentration are critical.

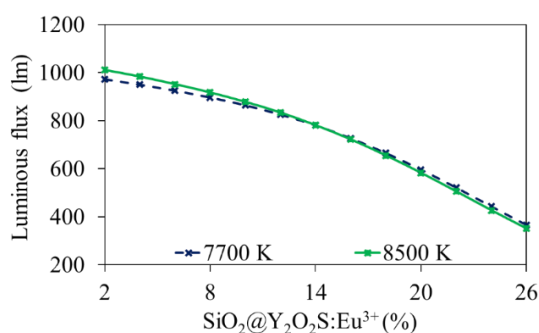


Figure 7. The illuminating beam of WLEDs and  $\text{SiO}_2@Y_2O_2S:Eu^{3+}$  concentration

#### 4. CONCLUSION

PMMA- $\text{SiO}_2$  nanocomposite is coated above the exterior of red phosphor  $Y_2O_2S:Eu^{3+}$  using sol-gel method with dip-coating technique followed by the reaction of MMA monomer and TEOS. The particle magnitude for nanoparticle  $\text{SiO}_2$  changes in connection with the reaction temperature. High temperature

(80 °C) reduced the particle size to 10 nm. The fluctuation in the size of SiO<sub>2</sub> particles also affects the scattering properties of the material. The bigger particle presents better scattering properties, according to the results obtained via Mie scattering theory. The impacts of SiO<sub>2</sub>@Y<sub>2</sub>O<sub>2</sub>S:Eu<sup>3+</sup> on the lighting performances of double-layer remote phosphor structure are investigated, regarding its concentration. The growth in SiO<sub>2</sub>@Y<sub>2</sub>O<sub>2</sub>S:Eu<sup>3+</sup> concentration significantly enhances either CRI or CQS. By using more than 20 %wt. SiO<sub>2</sub>@Y<sub>2</sub>O<sub>2</sub>S:Eu<sup>3+</sup>, peaks of CRI and CQS at approximately 85 and 74 can be accomplished, respectively. Nevertheless, the rise of SiO<sub>2</sub>@Y<sub>2</sub>O<sub>2</sub>S:Eu<sup>3+</sup> causes a considerable reduction in the luminous output of the package.

## ACKNOWLEDGEMENTS

This study was financially supported by Van Lang University, Vietnam.

## REFERENCES




- [1] A. S. Manikovskij, M. G. Komogorcev, and V. V. Stepanov, "The correction system for the direction of a locomotive spotlight's luminous flux," *IOP Conference Series: Materials Science and Engineering*, vol. 760, no. 1, p. 012042, 2020, doi: 10.1088/1757-899X/760/1/012042.
- [2] H. Sameshima *et al.*, "Mg ii and Fe ii Fluxes of Luminous Quasars at  $z \sim 2.7$  and the Evaluation of the Baldwin Effect in the Flux-to-abundance Conversion Method for Quasars," *The Astrophysical Journal*, vol. 904, no. 2, p. 162, 2020, doi: 10.3847/1538-4357/abc33b.
- [3] A. Sardinha, I. Ázara, M. Torres, and T. Menegotto, "Development of a LED based standard for luminous flux," *Journal of Physics: Conference Series*, vol. 975, no. 1, p. 012029, 2018, doi: 10.1088/1742-6596/975/1/012029.
- [4] P. N. Immanuel, C. C. Chiang, T. H. Lee, S. D. Midyeen, and S. J. Huang, "Utilization of Low Wavelength Laser Linking with Electrochemical Etching to Produce Nano-Scale Porous Layer on p-Type Silicon Wafer with High Luminous Flux," *ECS Journal of Solid State Science and Technology*, vol. 10, no. 1, p. 016003, 2021, doi: 10.1149/2162-8777/abdc4b.
- [5] A. Pons, J. Campos, and F. Sametoglu, "Bilateral comparison of luminous flux (EURAMET.PR-K4.3)," *Metrologia*, vol. 56, no. 1A, p. 02003, 2019, doi: 10.1088/0026-1394/56/1A/02003.
- [6] H. Y. Kim, J. M. Lee, K. M. Kang, and J. W. Lee, "Using Ag Sinter Paste to Improve the Luminous Flux and Reliability of InGaN-Based LED Package for Commercial Vehicle Daytime Running Light," *ECS Journal of Solid State Science and Technology*, vol. 10, no. 1, p. 015004, 2021, doi: 10.1149/2162-8777/abdc44.
- [7] A. Kokka *et al.*, "Validation of the fisheye camera method for spatial non-uniformity corrections in luminous flux measurements with integrating spheres," *Metrologia*, vol. 56, no. 4, p. 045002, Jun. 2019, doi: 10.1088/1681-7575/ab17fe.
- [8] J. Shin, T. Nagao, J. H. Woo, and H. A. N. Le, "The Fe ii/Mg ii Flux Ratio of Low-luminosity Quasars at  $z \sim 3$ ," *The Astrophysical Journal*, vol. 874, no. 1, p. 22, 2019, doi: 10.3847/1538-4357/ab05da.
- [9] Y. Nakazawa, K. Godo, K. Niwa, T. Zama, Y. Yamaji, and S. Matsuoka, "Establishment of  $2\pi$  total spectral radiant flux scale with a broadband LED-based transfer standard source," *Metrologia*, vol. 57, no. 6, p. 065024, 2020, doi: 10.1088/1681-7575/abba73.
- [10] H. Liu, Y. D. Lin, C. Z. Yang, and J. Yu, "APMP comparison on luminous flux units (APMP.PR-K4)," *Metrologia*, vol. 55, no. 1A, p. 02001, 2018, doi: 10.1088/0026-1394/55/1A/02001.
- [11] J. Dubard, G. Obein, and D. Suryani, "Bilateral comparison of luminous flux using lamps as transfer standards (EURAMET.PR-K4.2)," *Metrologia*, vol. 56, no. 1A, p. 02001, 2019, doi: 10.1088/0026-1394/56/1A/02001.
- [12] E. Setyaningsih, Y. Calvinus, and Y. A. Sabtalistia, "Analysis of LED Lumener for Street Lighting Based on lamp Housing, Drivers and Optics to get Luminous Efficacy," in *IOP Conference Series: Materials Science and Engineering*, vol. 1007, no. 1, p. 012041, Dec. 2020, doi: 10.1088/1757-899X/1007/1/012041.
- [13] W. Chen, X. Tang, Z. Zang, Y. Shi, Z. Yang, and J. Du, "Tunable dual emission in Mn<sup>2+</sup>-doped CsPbX<sub>3</sub> (X = Cl, Br) quantum dots for high efficiency white light-emitting diodes," *Nanotechnology*, vol. 30, no. 7, p. 075704, 2018, doi: 10.1088/1361-6528/aaf299.
- [14] M. Hämmer *et al.*, "Recyclable phosphor sheet based on polyvinyl alcohol for LED lighting using remote phosphor technology," *Materials Technology*, vol. 34, no. 3, pp.178-183, 2019, doi: 10.1080/10667857.2018.1541213.
- [15] H. Gauche *et al.*, "Screen Printing of Cotton Fabric with Hydrochromic Paste: Evaluation of Color Uniformity, Reversibility and Fastness Properties," *Journal of Natural Fibers*, pp. 1-12, 2020, doi: 10.1080/15440478.2020.1821288.
- [16] J. P. C. Nascimento, F. F. do Carmo, M. X. Façanha, S. J. T. Vasconcelos, J. C. Sales, and S. Sombra, "On the synthesis and down-conversion luminescence of the LaNbO<sub>4</sub>:Pr<sup>3+</sup> phosphor," *Ferroelectrics*, vol. 545, no. 1, pp. 55-61, 2019, doi: 10.1080/00150193.2019.1621711.
- [17] C. N. Liao, H. J. Chiu, and Y. C. Hsieh, "Wide-range dimmable LED lighting based on QL-SEPIC converter," *EPE Journal*, vol. 29, no. 1, pp. 25-37, 2019, doi: 10.1080/09398368.2018.1494671.
- [18] J. W. Han *et al.*, "Enhanced outcoupling in down-conversion white organic light-emitting diodes using imprinted microlens array films with breath figure patterns," *Science and Technology of Advanced Materials*, vol. 20, no. 1, pp. 35-41, 2019, doi: 10.1080/14686996.2018.1551040.
- [19] Z. Liu, Y. Liu, C. Pan, Y. Fang, and J. Hou, "K<sub>2</sub>MnF<sub>6</sub>/KHF<sub>2</sub> red phosphor synthesis by a low temperature way for high color rendering index white light emitting diodes," *Ferroelectrics*, vol. 565, no. 1, pp. 66-76, 2020, doi: 10.1080/00150193.2020.1761719.
- [20] D. Zhou, G. Yan, W. Zhang, J. Lin, and K. Qiu, "Synthesis and luminescence properties of Zn<sub>3</sub>B<sub>2</sub>O<sub>6</sub>:Eu<sup>3+</sup>, Li<sup>+</sup> red-emitting phosphor for white LEDs," *Ferroelectrics*, vol. 528, no. 1, pp.114-121, 2018, doi: 10.1080/00150193.2018.1448654.
- [21] M. Rajendran, K. Singh, and S. Vaidyanathan, "A novel Sm<sup>3+</sup>-activated Li<sub>3</sub>BaSrLn<sup>3</sup>(MO<sub>4</sub>)<sub>8</sub> [Ln = La, Gd, and Y; M = Mo and W] deep red-emitting phosphors for plant cultivation and white LEDs," *Journal of Information Display*, vol. 22, no. 2, pp. 63-81, 2021, doi: 10.1080/15980316.2020.1831630.
- [22] P. T. Tin, N. H. K. Nhan, T. H. Q. Minh, and N. T. P. Thao, "Red-emitting Ba<sup>2</sup>Si<sub>5</sub>N<sub>8</sub>Eu<sup>2+</sup> conversion phosphor: A new selection for enhancing the optical performance of the in-cup packaging MCW-LEDs," *Cogent Engineering*, vol. 5, no.1, p. 1486153, 2018,

doi: 10.1080/23311916.2018.1486153.




- [23] B. Deng, J. Chen, C. S. Zhou, dan H. Liu, "Synthesis and temperature-dependent optical properties of  $\text{Eu}^{3+}$ -doped  $\text{NaYSiO}_4$  red-emitting phosphors," *Integrated Ferroelectrics*, vol. 197, no. 1, pp. 77-82, 2019, doi: 10.1080/10584587.2019.1592084.
- [24] H. Xiea, C. Chen, J. Li, Y. He, and N. Wang, "Sol-gel synthesis and luminescent performance of  $\text{Eu}^{3+}$ ,  $\text{Lu}^{3+}$  co-doped  $\text{Ca}_{0.3}\text{Sr}_{0.7}\text{Mo}_{1-x}\text{W}_x\text{O}_4$  red-emitting phosphor," *Inorganic and Nano-Metal Chemistry*, vol. 51, no. 10, pp. 1297-1305, Oct. 2020, doi: 10.1080/24701556.2020.1835967.
- [25] S. Lee and H.C. Yoon, "LED lighting system for better color rendition space: the effect of color rendering index," *Journal of Asian Architecture and Building Engineering*, vol. 20, no. 5, pp. 556-565, 2020, doi: 10.1080/13467581.2020.1799801.

## BIOGRAPHIES OF AUTHORS



**Phuc Dang Huu**    received a Physics Ph.D degree from the University of Science, Ho Chi Minh City, in 2018. Currently, he is a lecturer at the Faculty of Fundamental Science, Industrial University of Ho Chi Minh City, Ho Chi Minh City, Vietnam. His research interests include simulation LEDs material and renewable energy. He can be contacted at email: danghuuphuc@iuh.edu.vn.



**Phan Xuan Le**    received a Ph.D. in Mechanical and Electrical Engineering from Kunming University of Science and Technology, Kunming city, Yunnan province, China. Currently, He is a lecturer at the Faculty of Engineering, Van Lang University, Ho Chi Minh City, Viet Nam. His research interests are optoelectronics (LED), power transmission and automation equipment. He can be contacted at email: le.px@vlu.edu.vn.